Journal of Magnetic Resonance **154,** 46–52 (2002)
doi:10.1006/jmre.2001.2461, available online at http://www.idealibrary.com on IDEAL®

Relative CSA–Dipolar Orientation from REDOR Sidebands

Robert D. O'Connor and Jacob Schaefer[1]

Department of Chemistry, Washington University, St. Louis, Missouri 63130

Received May 24, 2001; revised October 23, 2001

Algebraic expressions are given for the sideband intensities of REDOR dephasing experiments as a function of the relative orientation of the CSA and dipolar tensors. The expressions are straightforward to derive and implement and can be easily modified for variations in the spin systems, including distributions of distances and multiple dephasers. These expressions, along with the high sensitivity, resolution, and general robust nature of REDOR, make determining CSA–dipolar orientations from REDOR experiments reliable and, compared to full simulations, efficient and routine. Additionally, it is shown that even the ±1 sidebands of fast-spinning samples may contain significant information about orientation. Finally, numerical integration of the expressions supports the intuitive notion that any difference in the sideband dephasing rates is evidence of preferred CSA–dipolar orientations. This fact can be used to gauge the extent of local molecular order in intermolecular dephasing experiments.

INTRODUCTION

Many solid-state NMR techniques use the orientation dependence of anisotropic interactions to probe molecular order and orientation (*1–20*). Usually, these experiments correlate the orientation of a tensor quantity, such as the chemical shift anisotropy (CSA) or quadrupolar interaction, with either the magnetic field, $\boldsymbol{B}_0$, or with the orientation of another molecular tensor such as the CSA tensor of a different nucleus. Generally, the first type of correlation provides information about molecular order and the latter type provides information about inter- or intramolecular orientation.

Of the many anisotropic interactions, the magnetic dipolar interaction between two nuclei is particularly useful in that it is a function of both the internuclear distance and orientation. Potentially, a single experiment can yield both of these quantities. Additionally, the dipolar tensor has cylindrical symmetry and, consequently, requires only two Euler rotation angles to specify its orientation, as compared with three for a general second-rank tensor. This parameter reduction results in significant computational savings and easier visualization of the orientation because simpler spherical polar coordinates can be used.

[1] To whom correspondence should be addressed. E-mail: schaefer@wuchem.wustl.edu.

Many experiments have been proposed that correlate dipolar and CSA interactions to infer the relative orientation of their corresponding tensors (*4–6, 8–11, 14, 18–24*). One such experiment involves the REDOR dephasing of spinning sidebands (*9, 13, 19*). Along with the above advantages of the dipolar interaction, this experiment also has the advantages of high resolution and sensitivity, which are typical of 1-D, cross-polarization, magic-angle spinning experiments. Previously, simulations were used to determine the relative orientation (*9, 13, 19*). In the following, we will present algebraic expressions that can be used to calculate directly the REDOR sideband intensities and, then, illustrate their use in determining the relative orientation of a dipolar tensor with respect to a CSA tensor for L-[1-^{13}C,^{15}N]alanine.

THEORY

The CSA–dipolar orientation dependence for magic angle sample spinning (MAS) has been presented several times (*5, 6, 9, 25–27*). Heuristically, the dependence can be established by noting that sideband N is composed of its own CSA-weighted distribution, $G_N[\Omega]$, of CSA tensor orientations, where Ω represents the Euler powder angles (α, β, γ) describing the tensor orientation with respect to the rotor frame. This weighting, in conjunction with the orientation dependence of REDOR dephasing, $R_D[\Omega]$, embeds the relative CSA–dipolar tensor orientation into the sideband dephasing. From this view, the intensity of sideband N, I_N, should be an average of the form

$$I_N = \int R_D[\Omega; P_D] G_N[\Omega; P_{CS}] d\Omega, \qquad [1]$$

where P_{CS} and P_D represent general parameters describing the CSA and dipolar tensors, respectively. Below, such a relationship will be derived.

We begin by identifying the FID, $S[t]$, as

$$S[t] = \frac{1}{8\pi^2} \int d\Omega\, e^{i\Theta[t,\Omega,\delta,\eta,\alpha_D,\beta_D,D]}, \qquad [2]$$

where the instantaneous phase, Θ, is a result of both CSA (Θ_{CS}) and dipolar (Θ_D) evolution:

1090-7807/02 $35.00

$$\Theta[t, \Omega, \delta, \eta, \alpha_D, \beta_D, D] = \Theta_{CS}[t, \Omega, \delta, \eta] + \Theta_D[t, \Omega, \alpha_D, \beta_D, D]. \quad [3]$$

In these and following expressions, the parameters describing the tensors are: δ and η, the CSA anisotropy and asymmetry parameters; α_D and β_D, the azimuthal and polar angles of the dipolar vector in the CSA principal axis system, respectively; and, D, the dipolar coupling constant. Other parameter definitions include: ω_R, the rotor speed (rad/s); T_R the rotor period; B_R, the rotor angle with respect to $\boldsymbol{B}_0$ ($\tan^{-1}\sqrt{2}$ for MAS); t, the evolution time; ω_0, the Larmor frequency; and $\bar{\sigma}$, the isotropic chemical shift.

Θ_{CS} and Θ_D are given by

$$\Theta_{CS}[t, \Omega, \delta, \eta] = \int_0^t \omega_{CS}[\tau, \Omega, \delta, \eta]\, d\tau \quad [4]$$

$$\Theta_D[t, \Omega, \alpha_D, \beta_D, D] = \int_0^t \omega_D[\tau, \Omega, \alpha_D, \beta_D, D]\, d\tau, \quad [5]$$

where

$$\omega_{CS}(t, \Omega, \delta, \eta) = \sum_{q,q'=-2}^{2} \mathbf{A}_{2q'}^{CS_{PAS}}[\delta, \eta]\mathbf{D}_{q'q}^{2}[\alpha, \beta, \gamma] \times \mathbf{D}_{q0}^{2}[-\omega_R t, B_R, 0] + \omega_0\bar{\sigma} \quad [6]$$

and for spin $^1/_2$ nuclei

$$\omega_D[t, \Omega, \alpha_D, \beta_D, D] = \pm \sum_{q,q'=-2}^{2} \mathbf{A}_{20}^{D_{PAS}}[D]\mathbf{D}_{0q}^{2}[0, \beta_D, \pi - \alpha_D] \times \mathbf{D}_{qq'}^{2}[\alpha, \beta, \gamma]\mathbf{D}_{q'0}^{2}[-\omega_R t, B_R, 0]. \quad [7]$$

In Eqs. [6] and [7], the $\mathbf{D}_{nm}^{2}$ are the Wigner rotation matrices and the other tensors have typical definitions (*28*), which are stated explicitly in the Appendix.

The phase, Θ, is dependent on the pulse sequence, which in general will have two parts, REDOR evolution and free evolution (FID). The following derivation will be based on the sequence in Fig. 1, but, generally, it applies to any REDOR sequence that has the dephasing pulses separated by $T_R/2$. It should be noted that if antiphase components are neglected or eliminated (*9*), such pulse sequences generate real (absorptive/emissive) spectra (*29, 30*). During n rotor cycles of REDOR evolution, Θ_{CS} is refocused (i.e., $= 0$) and Θ_D evolves to

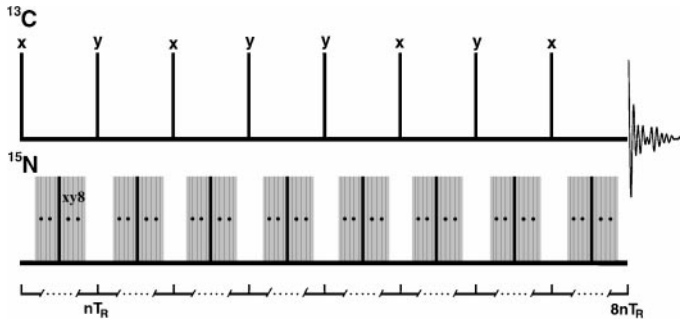

FIG. 1. Pulse sequence used for the REDOR experiments in which the number of ^{13}C pulses is fixed at eight in order to have both xy8 phase-cycling and minimal homonuclear effects. The gray boxes on the ^{15}N channel represent $(2n-1)$ xy8 phase-cycled π pulses every $^1/_2$ rotor cycle, where $n = 1, 2, 3, \ldots$. The total evolution time is, therefore, $n8T_R$. The S_0 spectra do not have ^{15}N pulses. ^1H CP generates the initial ^{13}C magnetization (not shown).

$$\Theta_D[\Omega, \alpha_D, \beta_D, \lambda_D] = n\left(\int_0^{T_R/2} \omega_D[\tau, \Omega, \alpha_D, \beta_D, D]\, d\tau - \int_{T_R/2}^{T_R} \omega_D[\tau, \Omega, \alpha_D, \beta_D, D]\, d\tau\right), \quad [8]$$

where λ_D equals $2\pi n D/\omega_R$, a unitless dipolar evolution parameter. The form of Θ_D after integration is given in the Appendix.

During the FID, there is Θ_{CS} evolution and, for simplicity, Θ_D is assumed to be zero. This assumption results in negligible error as long as $\delta \gg D$. Θ_{CS} during the FID is

$$\Theta_{CS}[t, \Omega, \delta, \eta] = \int_0^t d\tau\, \omega_{CS}[\tau, \Omega, \delta, \eta] = \omega_0\bar{\sigma}t + \omega_0(F_{CS}[\alpha, \beta, \gamma - \omega_R t, \delta, \eta] - F_{CS}[\alpha, \beta, \gamma, \delta, \eta]), \quad [9]$$

where F_{CS} is defined in the Appendix.

After inserting Eqs. [8] and [9] into Eq. [2], the sideband structure of the spectrum is apparent either by noting the periodicity of $S[t]$ and its Fourier series expansion (*25*) or by direct Fourier transformation of $S[t]$ (*31*). The Fourier transform is accomplished by first expanding the t-dependent trigonometric terms of $e^{i\Theta}$ into Bessel series. The transform is then straightforward and results in a $\delta[\omega_0\bar{\sigma} - \omega_R(j + l + 2k + 2m) - \omega]$ term in the spectrum, $S[\omega]$, where $\delta[x]$ represents the delta function with argument x; ω is the frequency (rad/s); and j, k, l, and m are the integer indices from the Bessel-series expansions. Setting N to $j + l + 2k + 2m$, this term mandates that there is only intensity at $\omega_0\bar{\sigma} - N\omega_R$ or integer multiples of ω_R from the isotropic

frequency. Explicitly, the intensity of the Nth sideband is

$$I_N[\delta, \eta, \alpha_D, \beta_D, \lambda_D] = \frac{1}{8\pi^2}\int d\Omega\Big[\exp(-i(F_{CS}[\alpha, \beta, \gamma, \delta, \eta] + \Theta_D[\alpha, \beta, \gamma, \alpha_D, \beta_D, \lambda_D] - N\gamma)) \cdot \sum_{klm=-\infty}^{\infty} e^{i\frac{\pi}{2}(l+m)} J^{A_1}_{N-l-2k-2m} J^{A_2}_k J^{B_1}_l J^{B_2}_m\Big], \quad [10]$$

where J^x_m represents an mth-order Bessel function of the first kind with argument x. The arguments are defined in the Appendix. Converting the series to an integral equation results in

$$I_N = \frac{1}{8\pi^2}\int d\Omega\left[e^{-i(F_{CS}[\alpha,\beta,\gamma,\delta,\eta]+\Theta_D[\alpha,\beta,\gamma,\alpha_D,\beta_D,\lambda_D]-N\gamma)} \frac{1}{2\pi}\int d\varphi e^{i(F_{CS}[\alpha,\beta,\varphi,\delta,\eta]-N\phi)}\right]. \quad [11]$$

Equation [11] is comparable to Eq. [1] with

$$G_N[\Omega; \delta, \eta] = e^{-i(F_{CS}[\alpha,\beta,\gamma,\delta,\eta]-N\phi)} \cdot \frac{1}{2\pi}\int d\varphi e^{i(F_{CS}[\alpha,\beta,\varphi,\delta,\eta]-N\gamma)} \quad [12]$$

and for the pulse sequence in Fig. 1

$$R_D[\alpha, \beta, \gamma; \alpha_D, \beta_D, \lambda_D] = \mathrm{Cos}[\Theta_D[\alpha, \beta, \gamma, \alpha_D, \beta_D, \lambda_D]], \quad [13]$$

where now both the $\pm$ spin states of the ensemble of dipolar interactions have been included. Thus,

$$I_N = \frac{1}{8\pi^2}\int d\Omega\, G_N[\Omega; \delta, \eta] R_D[\Omega; \alpha_D, \beta_D, \lambda_D]. \quad [14]$$

Assuming the integrals will be calculated numerically, Eqs. [12]–[14] provide an efficient means of calculating I_N because $G_N[\Omega; \delta, \eta]$ can be tabulated for each powder angle. Equation [14] also shows that only R_D must be calculated for other spin systems (such as spin 1 or multiple dephasers) and other pulse sequences. It should be noted, though, that this form of I_N is only valid if Θ_D and antiphase components are negligible during the FID (*9*).

EXPERIMENTS

The ^{13}C cross-polarization (CP) magic-angle spinning (MAS) spectra in Fig. 2 are of L-[1-^{13}C,^{15}N]alanine diluted 1 : 9 in

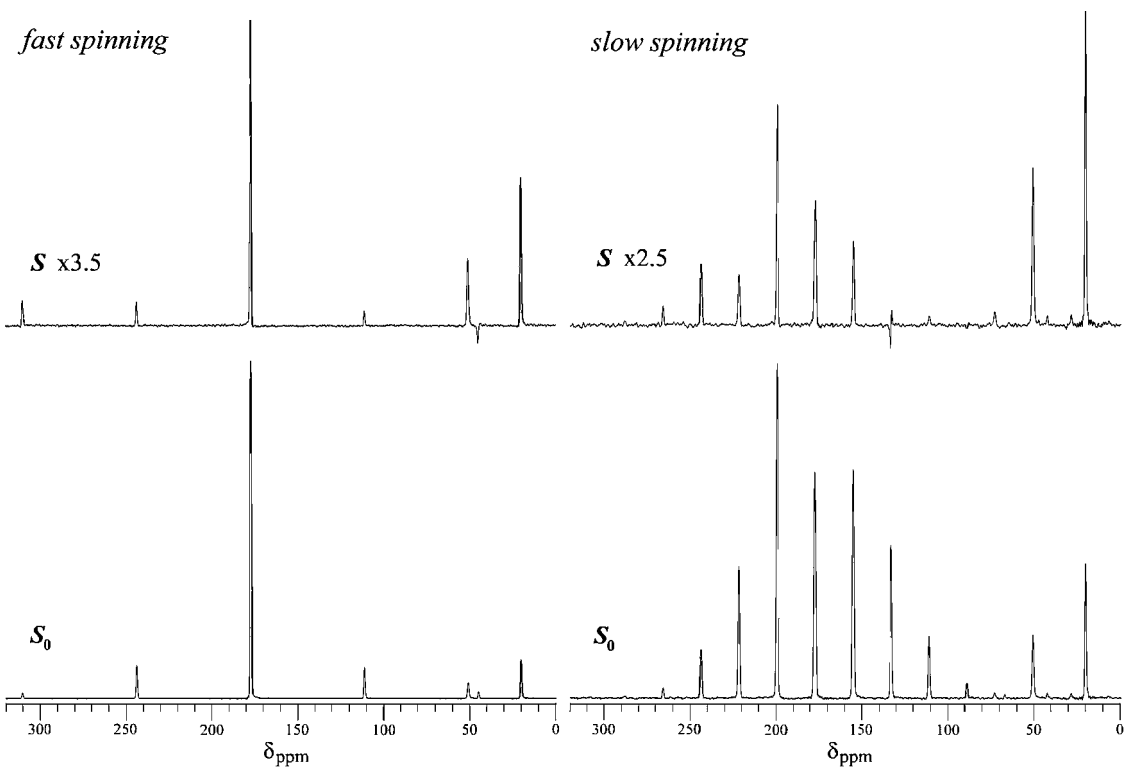

FIG. 2. ^{13}C{^{15}N} REDOR NMR spectra of diluted L-[1-^{13}C,^{15}N]alanine for an evolution time of 9.6 ms with $\omega_R/2\pi = 5000$ Hz (left) and $\omega_R/2\pi = 1667$ Hz (right). The bottom spectra are the S_0 reference spectra and the top are the S dephased spectra (with the stated vertical scale). At 1667 Hz, variations in sideband intensities of S relative to those of S_0 are apparent throughout the spectrum. For S at 5000 Hz, the variations are most apparent for the ± 2 sidebands. The resonances at 20 and 50 ppm are due to the natural-abundance methyl and α carbons, respectively.

natural abundance L-alanine and recrystallized. The spectra were acquired with a Chemagnetics CMX-300 spectrometer operating at 75.4532 MHz and ambient temperature using the pulse sequence in Fig. 1 and a probe described previously (*7*). Other experimental conditions included a 2-ms 50-kHz ^{13}C–^{1}H matched CP transfer, 50-kHz B_1 fields for the ^{13}C and ^{15}N π pulses, and 80-kHz proton decoupling. The S_0 and S spectra represent the reference (without ^{15}N pulses) and dephased (with ^{15}N pulses) spectra, respectively (*32*). The CSA parameters, δ and η, for the carboxyl carbon were obtained from a slow-spinning spectrum ($\omega_R/2\pi = 1000$ Hz, not shown) and found to be 5265 Hz and 0.79, respectively (*31*, *33*, *34*). From the REDOR spectra with $\omega_R/2\pi = 1667$ Hz, D was found to be 182 Hz (*35*).

RESULTS

Typical REDOR spectra of diluted L-[1-^{13}C,^{15}N]alanine are shown in Fig. 2. The differences in the sideband dephasing rates are most apparent in the 1667-Hz spectra and the ± 2 sidebands of the 5000-Hz spectra. Figure 3 shows the experimental (symbols) and calculated (curves) centerband and ± 1 sideband dephasing, $\Delta S/S_0$, where $\Delta S = (S_0 - S)$, as a function of the REDOR evolution time for $\omega_R/2\pi = 5000$ Hz. Differences in dephasing rates are obvious. To account for experimental factors such as finite pulses, incomplete decoupling, etc., and to allow for a more accurate visual comparison of the experimental and calculated sideband dephasing rates, the data were scaled so that the sum of the sideband and centerband dephasing, i.e., the total dephasing, matched the corresponding theoretical values for a 182-Hz coupling. This scaling predominantly affected the data around 9.6 ms, which only reached about 0.9 for both the 1667 and 5000-Hz data after being corrected for natural abundance contributions to S_0. This scaling was also applied while determining the best fit for the relative CSA–dipolar orientation, but intensity ratios with no scaling, could have been used with equal effectiveness. The curves in Fig. 3 were generated using Eqs. [12]–[14] with $\alpha_D = 27^\circ$, $\beta_D = 80^\circ$, and the other parameters as stated previously.

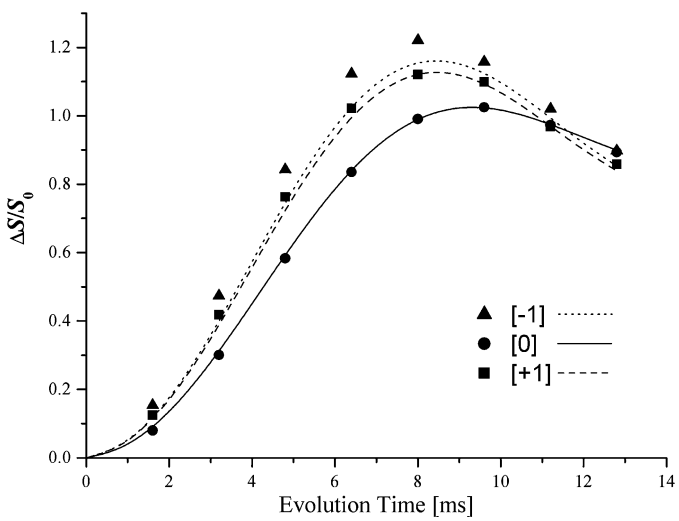

FIG. 3. Experimental (symbols) and calculated (curves) REDOR sideband dephasing ($\Delta S/S_0$) as a function of the dipolar evolution time for $\omega_R/2\pi = 5000$ Hz. The experimental values have been scaled so that the total dephasing at each evolution time equals that of the calculation. The calculations are based on a CSA-dipolar orientation of $\alpha_D = 27^\circ$ and $\beta_D = 80^\circ$ and CSA parameters $\delta = 5265$ Hz and $\eta = 0.79$.

The contour plots in Fig. 4 illustrate the sideband dephasing as a function of α_D and β_D for $\lambda_D = 1.75$, which corresponds to the 9.6-ms data in Fig. 3. The plots show the D_{2h} symmetry of the relative CSA–dipolar orientations where $\{\alpha_D, \beta_D\} = \{-\alpha_D, \beta_D\} = \{\pi - \alpha_D, \beta_D\} = \{\alpha_D, \pi - \beta_D\} = \{\pi - \alpha_D, \pi - \beta_D\} = \{\pi + \alpha_D, \pi - \beta_D\} = \{-\alpha_D, \pi - \beta_D\} = \{\pi + \alpha_{D,} \beta_D\}$, which results from an assumed symmetric CSA tensor. Figure 5 is a contour plot of the $0^\circ < \alpha_D, \beta_D < 90^\circ$ region of the error function, χ^2, as a function of orientation using the 4.8- and 9.6-ms data with $\omega_R/2\pi = 5000$ Hz. χ^2 is defined as

$$\chi^2[\alpha_D, \beta_D, \lambda_D] = \sqrt{\sum_{j,k}(1 - S^k[\lambda_D]_{exp(j)}/S^k[\alpha_D, \beta_D, \lambda_D]_{calc(j)})^2}, \quad [15]$$

where S^k is the integrated (scaled) intensity of the kth sideband ($k = -1 \cdots +1$) and $exp(j)$ and $calc(j)$ denote experimental (scaled) and calculated values, respectively, for the jth dephasing time.

Figure 6 shows the scaled REDOR data (symbols) and corresponding calculations for the upper sidebands and centerband with $\omega_R/2\pi = 1667$ Hz. The analysis was performed as described for the 5000-Hz data. Figure 7 shows the lower sidebands and corresponding calculation for the 1667-Hz data. Figure 8 shows the χ^2 plot that results from the 4.8 and 9.6 ms data with $\omega_R/2\pi = 1667$ Hz and $k = -3 \ldots +3$.

DISCUSSION

Compared to density matrix simulations (*13*), Eqs. [12]–[14] allow for a quicker, less tedious analysis of sideband data. From a data-processing perspective, this approach does not require a multitude of simulated spectra to analyze. Although the contour plots in Fig. 4, or complimentary plots of the ratios of S^i/S_0^i to S^j/S_0^j, could be used in a graphical analysis, such as that used by Herzfeld and Berger (*31*), to determine the relative orientation, the REDOR sideband analysis is more practical, efficient, and automated if χ^2 is used in either a search procedure, as we have done, or in a minimization routine (*36*). Additionally, the error function can be easily manipulated to include data and calculations from multiple REDOR evolution times (i.e., varying λ_D), sideband ratios, etc.

In the analysis of the relative CSA–dipolar orientation for the intramolecular interaction in alanine, there are five variables

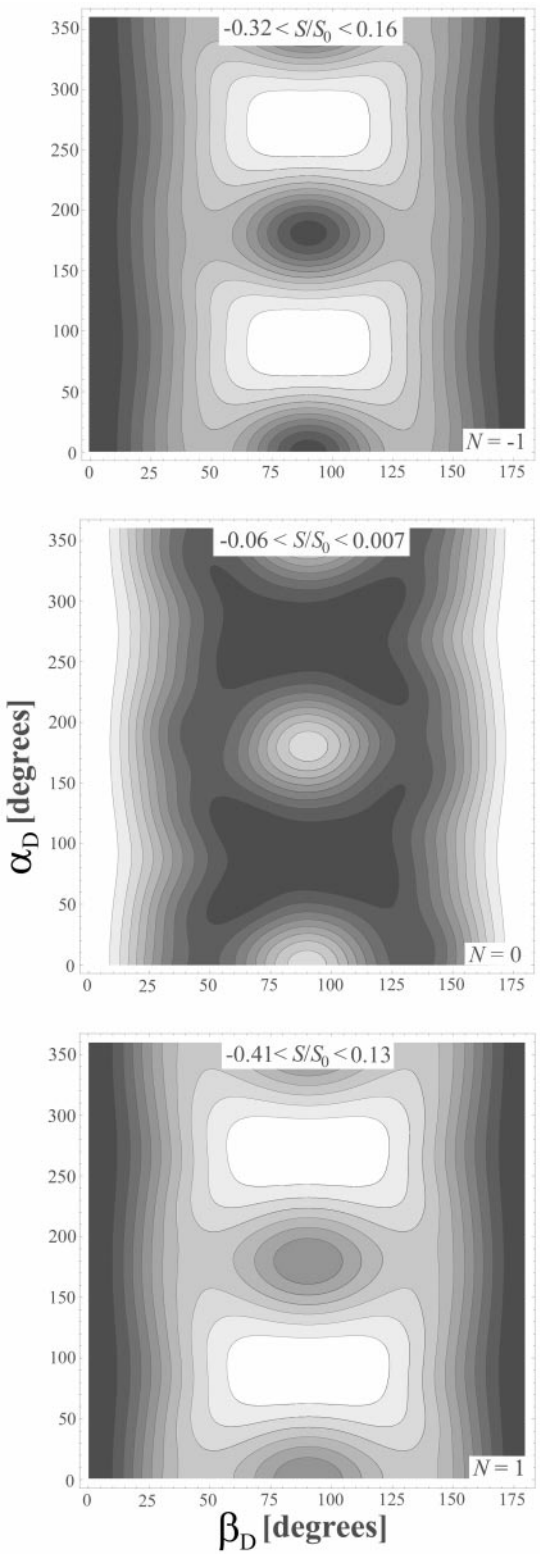

FIG. 4. S/S_0 contour plots of the -1, 0, and $+1$ sidebands as a function of polar angles α_D and β_D. For the plots, $\lambda_D = 1.75$ and $\omega_R/2\pi = 5000$ Hz. The contours divide the range between the minimum and maximum calculated values (shown on the plots) into 10 equally spaced intervals with the darkest region corresponding to the smallest S/S_0 or greatest dephasing.

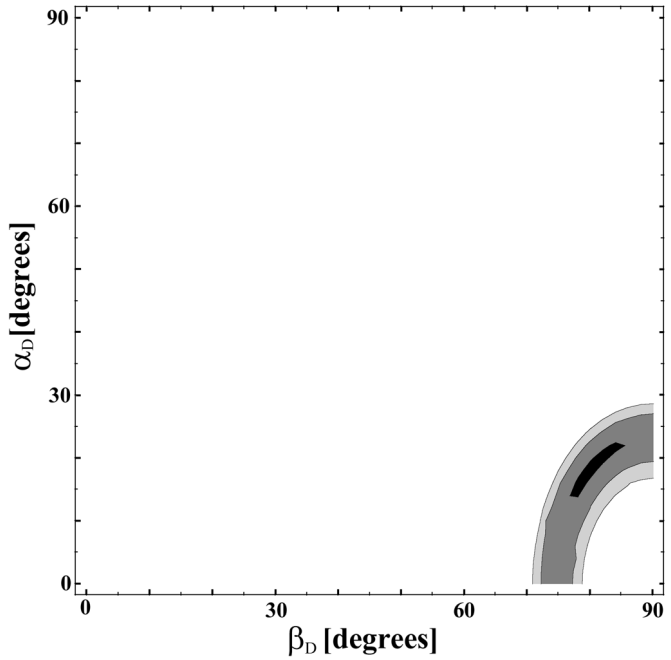

FIG. 5. Contour plot of the minimum χ^2 values for the 5000-Hz REDOR data as a function of the angles α_D and β_D. Each contour represents a 50% increase in error (χ^2), with the darkest region representing the best fit.

(Eq. [14]). The only parameters external to the REDOR experiment are the CSA anisotropic and asymmetry values, which are relatively straightforward to determine (*31*, *33*). The dipolar coupling can be derived from the REDOR data independently from the orientation (*32*), leaving only α_D and β_D, the angles describing the relative CSA–dipolar orientation,

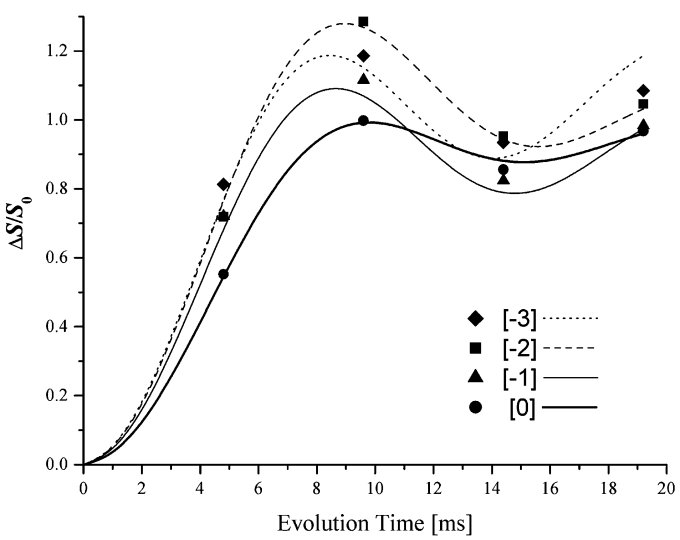

FIG. 6. Experimental (symbols) and calculated (curves) REDOR sideband dephasing ($\Delta S/S_0$) as a function of evolution time for the upper sidebands at $\omega_R/2\pi = 1667$ Hz. The scaling and calculation are similar to that of Fig. 3.

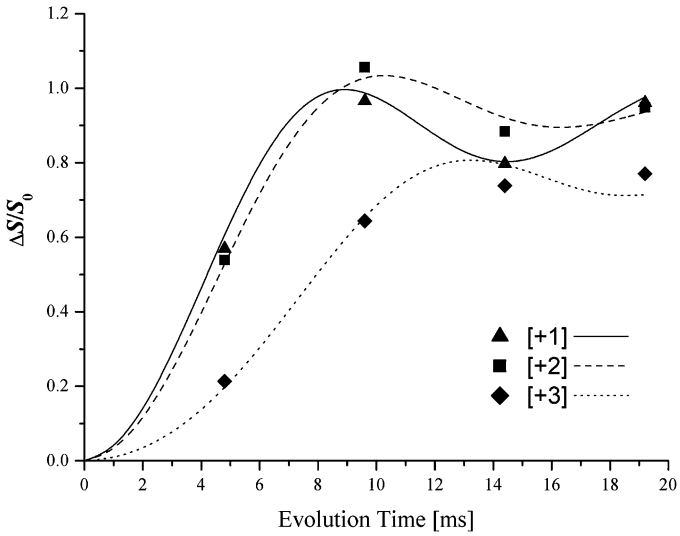

FIG. 7. Experimental (symbols) and calculated (curves) REDOR sideband dephasing as a function of evolution time for the lower sidebands at $\omega_R/2\pi =$ 1667 Hz. The scaling and calculation are similar to those of Fig. 3.

to be derived from the sideband data. Of course, to relate the dipolar orientation to the molecular frame, the orientation of the CSA principal axis would also have to be known in this frame.

The orientations that reproduce the experimental dephasing rates are shown in χ^2 plots of Figs. 5 and 8. The plot for the 5000-Hz data shows that even limited data can significantly reduce the parameter space of the probable orientations. Thus, if sensitivity is limiting, significant orientation information may be derived from fast-spinning experiments. Of course, spinning slower results in more distinguishable $G_N[\Omega, \delta, \eta]$s and, consequently, the range of probable orientations will be reduced. The χ^2 plot in Fig. 8 shows that spinning L-[1-^{13}C,^{15}N] alanine at 1667 Hz reduced the probable orientations significantly from the 5000-Hz data to a narrow region centered at $\{27^\circ, 80^\circ\}$. In a single crystal study, the orientation was reported to be $\{23^\circ, 79^\circ\}$ (*37*).

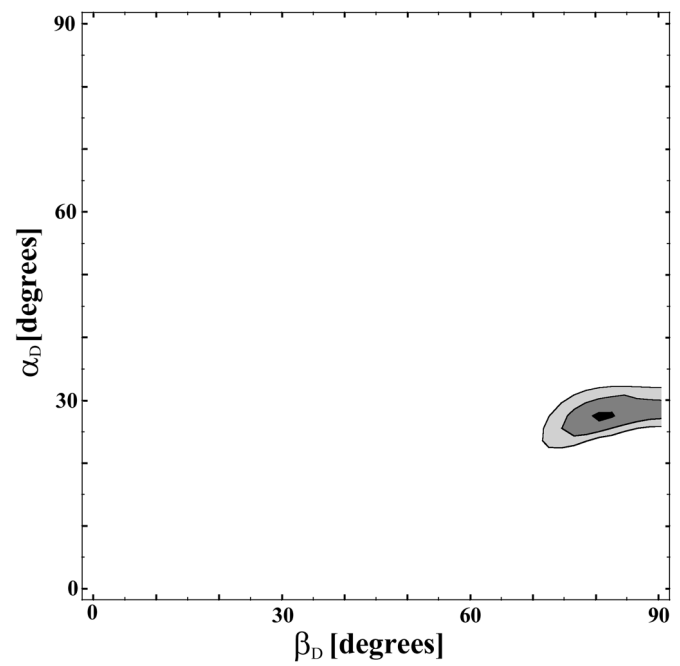

FIG. 8. Contour plot of the minimum χ^2 values for the 1667-Hz REDOR data as a function of the angles α_D and β_D. Each contour represents a 50% increase in error, with the darkest region representing the best fit.

Although not pertinent to alanine, a simple and important aspect of sideband dephasing is that for an isotropic distribution of CSA–dipolar orientations, all sidebands will dephase at the same rate. This assertion seems intuitively clear, but we confirmed it by numerically integrating Eq. [14] over an isotropic distribution of orientations. Thus, without further analysis, sideband dephasing plots such as those of Figs. 3, 6, and 7 indicate whether there are preferred CSA–dipolar orientations in powder samples. For intermolecular interactions in seemingly amorphous systems such as polymer glasses, such plots, or even a single REDOR dephased spectrum, may be very useful for determining the presence of microscopic local order.

APPENDIX

$$\Omega \Rightarrow \alpha, \beta, \gamma \qquad B_R = \mathrm{Tan}^{-1}[\sqrt{2}] \qquad \omega_0 = -\gamma_n \mathbf{B}_0$$

$$\bar{\sigma} = \frac{\sigma_{xx} + \sigma_{yy} + \sigma_{zz}}{3} \qquad \delta = \sigma_{zz} - \bar{\sigma} \qquad \eta = \frac{\sigma_{yy} - \sigma_{xx}}{\delta}$$

$$\mathbf{A}_{20}^{\mathrm{CS_{PAS}}} = -\omega_0 \delta \qquad \mathbf{A}_{2\pm2}^{\mathrm{CS_{PAS}}} = -\omega_0 \delta \eta/\sqrt{6} \qquad \mathbf{A}_{2\pm1}^{\mathrm{CS_{PAS}}} = 0$$

$$D = \frac{\gamma_{1n}\gamma_{2n}\hbar}{2\pi r^3} \qquad \mathbf{A}_{20}^{\mathrm{D_{PAS}}} = D \qquad \lambda_D = nT_R D \qquad \text{[A1]}$$

$$A_1[\alpha, \beta, \delta, \eta] = \frac{\delta\sqrt{2}}{2\omega_R} \mathrm{Sin}\, 2\beta \left(\frac{\eta}{3} \mathrm{Cos}\, 2\alpha + 1 \right) \qquad \text{[A2]}$$

$$A_2[\alpha, \beta, \delta, \eta] = \frac{\delta}{4\omega_R} \left(\frac{\eta}{3} (\mathrm{Cos}^2\beta + 1) \mathrm{Cos}\, 2\alpha - \mathrm{Sin}^2\, \beta \right) \qquad \text{[A3]}$$

$$B_1[\alpha, \beta, \delta, \eta] = \frac{\delta\eta\sqrt{2}}{3\omega_R} \mathrm{Sin}\, 2\alpha\, \mathrm{Sin}\, \beta \qquad \text{[A4]}$$

$$B_2[\alpha, \beta, \delta, \eta] = \frac{\delta\eta}{6\omega_R} \mathrm{Sin}\, 2\alpha\, \mathrm{Cos}\, \beta \qquad \text{[A5]}$$

$$\begin{aligned} F_{CS}[\alpha, \beta, \gamma, \delta, \eta] &= \omega_0 (A_1[\alpha, \beta, \delta, \eta] \mathrm{Sin}[\gamma] + A_2[\alpha, \beta, \delta, \eta] \mathrm{Sin}[2\gamma] \\ &\quad + B_1[\alpha, \beta, \delta, \eta] \mathrm{Cos}[\gamma] + B_2[\alpha, \beta, \delta, \eta] \mathrm{Cos}[2\gamma]) \end{aligned} \qquad \text{[A6]}$$

$$C_1[\alpha, \beta, \alpha_D, \beta_D, \lambda_D] = \lambda_D\sqrt{2}\Big(2\mathrm{Sin}\,2\beta_D\,\mathrm{Cos}\,2\beta\,\mathrm{Cos}\,(\alpha-\alpha_D) + \mathrm{Sin}^2\,\beta_D\,\mathrm{Sin}\,2\beta\,\mathrm{Cos}\,2(\alpha-\alpha_D) - \frac{1}{2}(1+3\mathrm{Cos}\,2\beta_D)\mathrm{Sin}\,2\beta\Big) \quad [A7]$$

$$D_1[\alpha, \beta, \alpha_D, \beta_D, \lambda_D] = \lambda_D 2\sqrt{2}(\mathrm{Sin}^2\,\beta_D\,\mathrm{Sin}\,\beta\,\mathrm{Sin}\,2(\alpha-\alpha_D) + \mathrm{Sin}\,2\beta_D\,\mathrm{Cos}\,\beta\,\mathrm{Sin}\,(\alpha-\alpha_D)) \quad [A8]$$

$$\Theta_D[\alpha, \beta, \gamma, \alpha_D, \beta_D, \lambda_D] = C_1[\alpha, \beta, \alpha_D, \beta_D, \lambda_D]\mathrm{Cos}\,\gamma + D_1[\alpha, \beta, \alpha_D, \beta_D, \lambda_D]\mathrm{Sin}\,\gamma \quad [A9]$$

ACKNOWLEDGMENT

This work was supported by NIH Grant GM51554.

REFERENCES

1. D. P. Weliky and R. Tycko, *J. Am. Chem. Soc.* **118,** 8487–8488 (1996).
2. R. Tycko, D. P. Weliky, and A. E. Berger, *J. Chem. Phys.* **105,** 7915 (1996).
3. K. Schmidt-Rohr, *Macromolecules* **29,** 3975 (1996).
4. P. Palmas, P. Tekely, and D. Canet, *J. Magn. Reson. Ser. A* **104,** 26–36 (1993).
5. P. Palmas, C. Malveau, P. Tekely, and D. Canet, *Solid State NMR* **13,** 45–53 (1998).
6. M. G. Munowitz and R. G. Griffin, *J. Chem. Phys.* **76,** 2848 (1982).
7. B. D. Mueller, A. Schmidt, K. L. Pappan, R. A. McKay, and J. Schaefer, *Biochemistry* **34,** 5597 (1995).
8. J. Leppert, B. Heise, and R. Ramachandran, *J. Biomolecular NMR* **18,** 153–164 (2000).
9. J. Leppert, B. Heise, and R. Ramachandran, *J. Magn. Reson.* **145,** 307–314 (2000).
10. Y. Ishii, T. Terao, and M. Kainosho, *Chem. Phys. Lett.* **256,** 133–140 (1996).
11. M. Hong, J. D. Gross, C. M. Rienstra, R. G. Griffin, K. K. Kumashiro, and K. Schmidt-Rohr, *J. Magn. Reson.* **129,** 85–92 (1997).
12. R. A. Haberkorn, R. E. Stark, H. v. Willigin, and R. G. Griffin, *J. Am. Chem. Soc.* **103,** 2534–2539 (1981).
13. J. M. Goetz and J. Schaefer, *J. Magn. Reson.* **129,** 222–223 (1997).
14. T. Fujiwara, T. Shimomura, and H. Akutsu, *J. Magn. Reson.* **124,** 147–153 (1997).
15. X. Feng, Y. K. Lee, D. Sandström, M. Edén, M. H. A. Sebald, and M. H. Levitt, *Chem. Phys. Lett.* **257,** 314–320 (1996).
16. R. R. Ernst, G. Bodenhausen, and A. Wokaun, "Principles of Nuclear Magnetic Resonance in One and Two Dimensions," Vol. 14, Oxford University Press, New York (1991).
17. G. Dabbagh, D. P. Weliky, and R. Tycko, *Macromolecules* **27,** 6183–6191 (1994).
18. J. Leppert, B. Heise, and R. Ramachandran, *Solid State NMR* **19,** 1–18 (2001).
19. B. Heise, J. Leppert, and R. Ramachandran, *Solid State NMR* **16,** 177–187 (2000).
20. J. Herzfeld, and R. G. Griffin, *J. Chem. Phys.* **86,** 597–602 (1987).
21. J. E. Roberts, G. S. Harbison, M. G. Munowitz, J. Herzfeld, and R. G. Griffin, *J. Am. Chem. Soc.* **109,** 4163–4169 (1987).
22. P. Tekely, F. Montigny, D. Canet, and J. J. Delpuech, *Chem. Phys. Lett.* **175,** 401 (1990).
23. J. Boisbouvier, B. Brutscher, A. Pardi, D. Marion, and J. P. Simorre, *J. Am. Chem. Soc.* **122,** 6779 (2000).
24. Y. F. Wei, D. K. Lee, and A. Ramamoorthy, *Chem. Phys. Lett.* **324,** 20–24 (2000).
25. O. N. Antzutkin, *Progr. NMR Spectrosc.* **35,** 203–266 (1999).
26. P. Tekely, *Solid State NMR* **14,** 33–41 (1999).
27. M. Linder, A. Höhener, and R. R. Ernst, *J. Chem. Phys.* **73,** 4959 (1980).
28. U. Haeberlen, "High Resolution NMR in Solids—Selective Averaging," Vol., Supplement 1, Academic Press, New York (1976).
29. T. Gullion and M. S. Conradi, *J. Magn. Reson.* **86,** 39–45 (1990).
30. M. H. Levitt, *J. Magn. Reson.* **83,** 427–433 (1989).
31. J. Herzfeld and A. E. Berger, *J. Chem. Phys.* **73,** 6021 (1980).
32. T. Gullion and J. Schaefer, *J. Magn. Reson.* **81,** 196–200 (1989).
33. M. Levitt and Y. K. Lee, http://www.fos.su.se/physical/mhl/index.html (2000).
34. P. Hodgkinson and L. Emsley, *J. Chem. Phys.* **107,** 4808 (1997).
35. T. Gullion and J. Schaefer, *Adv. Magn. Reson.* **13,** 57 (1989).
36. "Mathematica," computer program for calculating sideband intensities, available at: http://www.chemistry.wustl.edu/Faculty/Schaefer/index.html.
37. A. Naito, S. Ganapathy, K. Akasaka, and C. A. McDowell, *J. Chem. Phys.* **74,** 3190 (1981).